SOURCE PROCESS OF THE 2006 OITA-CHUBU EARTHQUAKE (M_W6.4) OCCURRING IN THE PHILIPPINE SEA SLAB

H. Nagumo[1] and T. Sasatani[2]

[1] *Research student, Graduate School of Engineering, Hokkaido University, Sapporo. Japan*
[2] *Professor, Graduate School of Engineering, Hokkaido University, Sapporo, Japan*
Email: nagumo@eng.hokudai.ac.jp, sasatani@eng.hokudai.ac.jp

ABSTRACT :

We investigate source characteristics of a moderate-size intermediate-depth earthquake (M_W6.4) occurring on 12 June, 2006 at a depth of about 145km in the Philippine Sea slab subducting beneath the Kyushu district, Japan. First we investigate rupture process from waveform inversion of strong ground motion and teleseismic body wave data. The result shows complex source process of this earthquake. We extract two asperities form the inversion result. Next we estimate the short period level of S-wave acceleration source spectrum. Estimated short period level is consistent with typical level estimated from other intraslab events, which is higher than that of crustal and interplate earthquake.

KEYWORDS: 2006 Oita-chubu earthquake, intraslab earthquake, waveform inversion, spatio-temporal slip distribution, asperity model

1. INTRODUCTION

A moderate-size intraslab earthquake occurred on 12 June, 2006 in the Philippine Sea plate beneath central Oita prefecture, Kyushu, Japan. We call this event the 2006 Oita-chubu earthquake. The Harvard mechanism solution shows a down-dip extension focal mechanism. The JMA focal depth is 145.1 km that corresponds to the deepest portion of a vertical deep-seismic zone (Fig. 1). Source parameters are listed in Table 1. Since the aftershock activity of the 2006 Oita-chubu earthquake is very low, it is difficult to select fault plane from the two nodal planes based on the aftershock distribution.

In this region intraslab earthquake greater than moderate size is seldom occurred. In Japan, high density strong motion observation network system is constructed by National Research Institute for Earth Science and Disaster Prevention (Okada *et al*., 2004). Large numbers of high quality digital strong motion data were recorded during this event. Then it is a good opportunity to study source characteristics occurring in the Philippine Sea plate.

On the other hand, after the 1993 Kushiro-Oki earthquake, intraslab earthquakes are recognized to be one of the earthquake categories which can cause serious earthquake disasters. Moreover resent studies show the short period level of S-wave acceleration source spectrum of this category is higher than that of other categories (Maeda, 2003; Morikawa and Sasatani, 2004; Satoh, 2004). It is important to investigate source characteristics of intraslab earthquakes for mitigation of earthquake disasters.

In this study we perform waveform inversion to estimate spatio-temporal slip distribution during the 2006 Oita-chubu earthquake. In the inversion we use strong motion data obtained by NIED and teleseismic body wave data obtained by IRIS-DMC, simultaneously. Next we estimate the short period level of this earthquake.

Table 1.1 Source parameters used in this study

Latitude*	Longitude*	Depth*	Strike**	Dip**	Rake**
33.1353	131.4355	145.1km	45/181	67/30	110/51

*Determined by JMA, **Determined by Harvard University

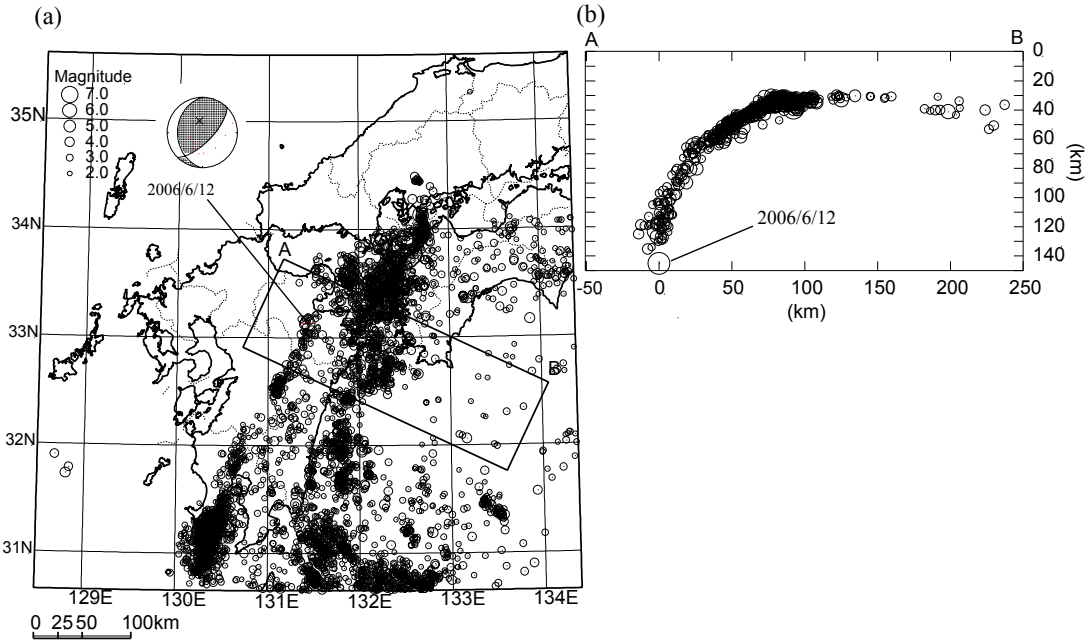

Figure 1 (a) Seismic activity of earthquakes greater than M_{JMA}2.0 in the Kyushu district from 1999 to 2006 and (b) vertical cross section within rectangular area in Fig. 1(a). Hypocenters are plotted in the depth range of 20 to 150 km.

2. FEATURE OF OBSERVED WAVEFORMS

Waveform data contain source, path and site effects. We try to get some information about the source from observed waveforms. Figure 2a shows S-wave portion of displacement waveforms at strong motion sites located near two nodal planes. They are low pass filtered at 0.7 Hz cutoff. These displacement waveforms are integrated twice from acceleration record. During the integration, high pass filter at 0.1 Hz cutoff is applied. We can see at least two S-wave pulses. This indicates the source contains at least two asperities. It is clear that the pulse width changes more drastically at sites near the eastern dipping nodal plane. This suggests that rupture propagates on the eastern dipping nodal plane. The pulse width also indicates rupture propagate to shallower direction from the hypocenter. Figure 2b shows P-wave portion of the UD component at teleseismic sites. P-wave ripples at SFJD suggest that rupture did not smoothly propagate. The P-wave pulse width also suggests that source process time is about 6 sec.

3. WAVEFORM INVERSION

3.1. Inversion Method

We estimate spatio-temporal slip distribution on the fault plane from waveform inversion. Multi-time window analysis (Hartzell and Heaton, 1983) is applied to both strong motion and teleseismic body wave data. We use velocity waveform. In the strong motion dataset, we use S-wave portion of two horizontal components, on the other hand, we use P-wave portion of UD component from the teleseismic data. Time length of 12 sec containing main phase is used for the inversion. Each dataset is re-sampled with a sampling interval of 0.05 sec. Low-pass filtered at 1 Hz cutoff is applied to only strong motion data. We assume a single fault plane of eastern dip. The fault segment is divided into 2 x 2 km^2 sub-faults for the waveform inversion. The number of sub-faults along strike is 9 and that along dip direction is 10. Total fault size is determined by preliminary analysis, which is the smallest one not to concentrate large slip near the fault edge. The number of time

windows is six. Each time window has duration of 0.6 sec and one time window is put after the previous one with a time lag of 0.3 sec. In general, an increase in the number of model parameters may lead to instability of the solution. To obtain more stable results, we applied smoothing constraints to the slip distribution with respect to time and space and to determine the smoothness parameter objectively, we adopted the optimized Akaike's Bayesian information criterion (ABIC; Akaike, 1980), which was developed by Fukahata *et al.* (2004). The Green's function is calculated by discrete wave number method (Bouchon, 1981; Takeo, 1985) for the strong motion sites and by linear filter theory by convolution of source, path and site factors for teleseismic sites (Kanamori and Stwart, 1976). We assume proper subsurface structure model based on geophysical exploration results for calculation of the Green's function at strong motion sites and JB model for teleseismic sites. Figure 3 shows site locations used in this analysis.

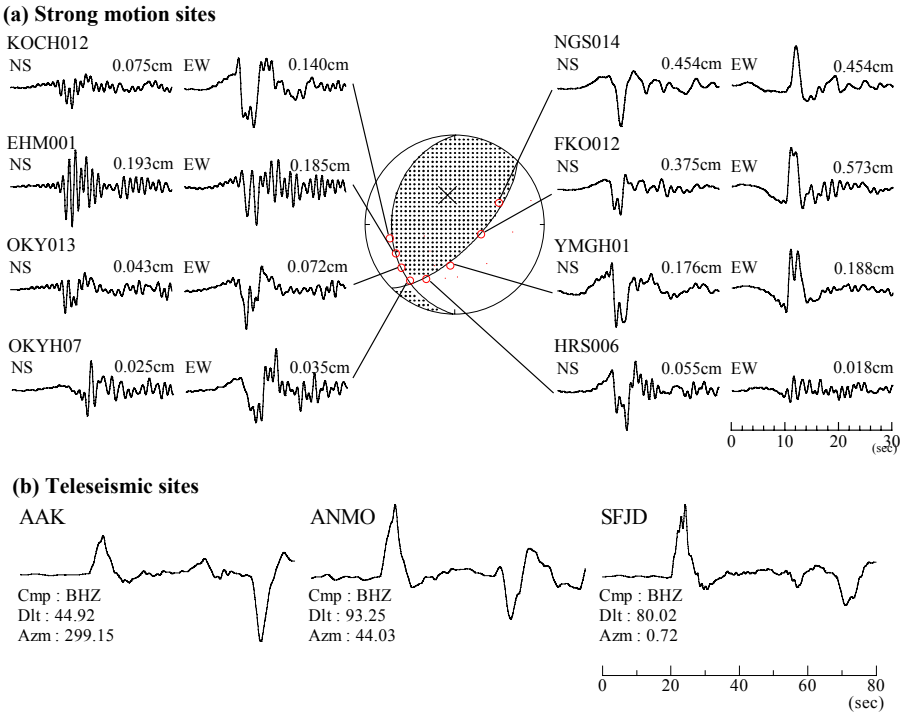

Figure 2. (a) Focal mechanism of the 2006 Oita-chubu earthquake projected on the lower hemisphere and displacement waveforms of S-wave portion observed at strong motion sites located near the two nodal planes. Each trace is low pass filtered at 1 Hz cutoff. Maximum amplitudes are indicated above each trace. (b) Displacement waveforms of P-wave portion observed at teleseismic sites.

3.2. Results

Figure 4 shows the comparison between the observed waveforms and the synthetic waveforms obtained from the inversion. Waveform fitting is quite well both at strong motion sites and teleseismic sites. Figure 5 shows inversion results. Total seismic moment is 3.42 x 10^{18} Nm. This value is slightly smaller than that of Harvard solution. Moment rate function is calculated by summing up all resultant moment rate functions at each sub-fault (Fig. 5a). Total source process time is about 6 sec. We can see 4 pulses in the moment rate function, which suggest the complexity of the process. Resultant source mechanism is coincident with the Harvard solution (Fig. 5b). In Figure 5c we can see at least two portions with larger slip in the fault; one is just above the hypocenter and the other is apart about 8 km toward shallower direction from the hypocenter. The maximum slip is about 70 cm. Relatively large slip portions can also be seen near the fault edge. Some of them may be artificially produced by error of assumed velocity model and uncertainty like lateral heterogeneity of the actual structure.

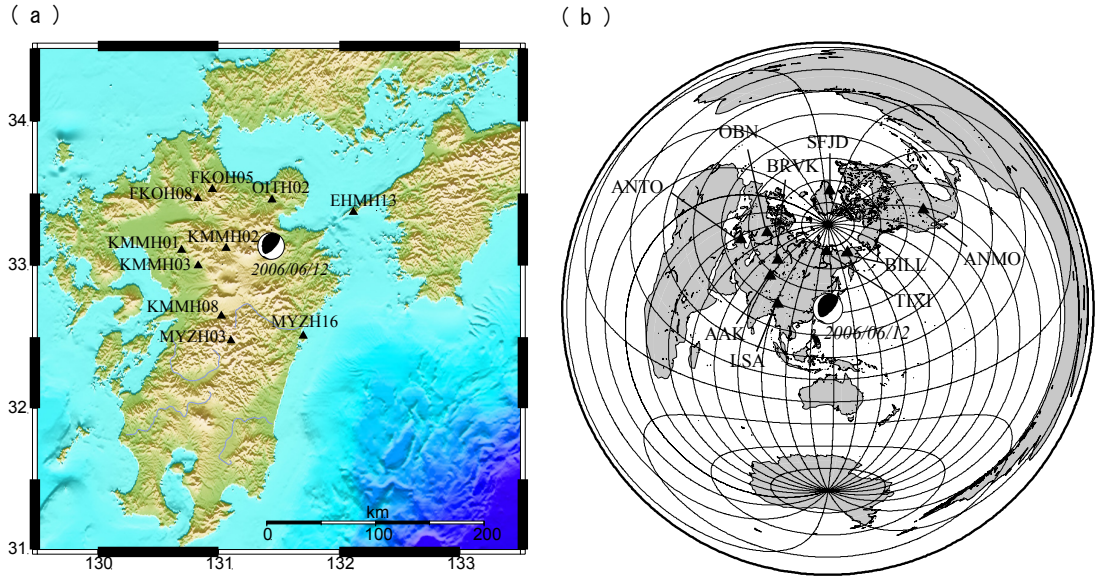

Figure 3 Site locations used in source process analysis. (a) Strong motion sites and (b) teleseismic sites.

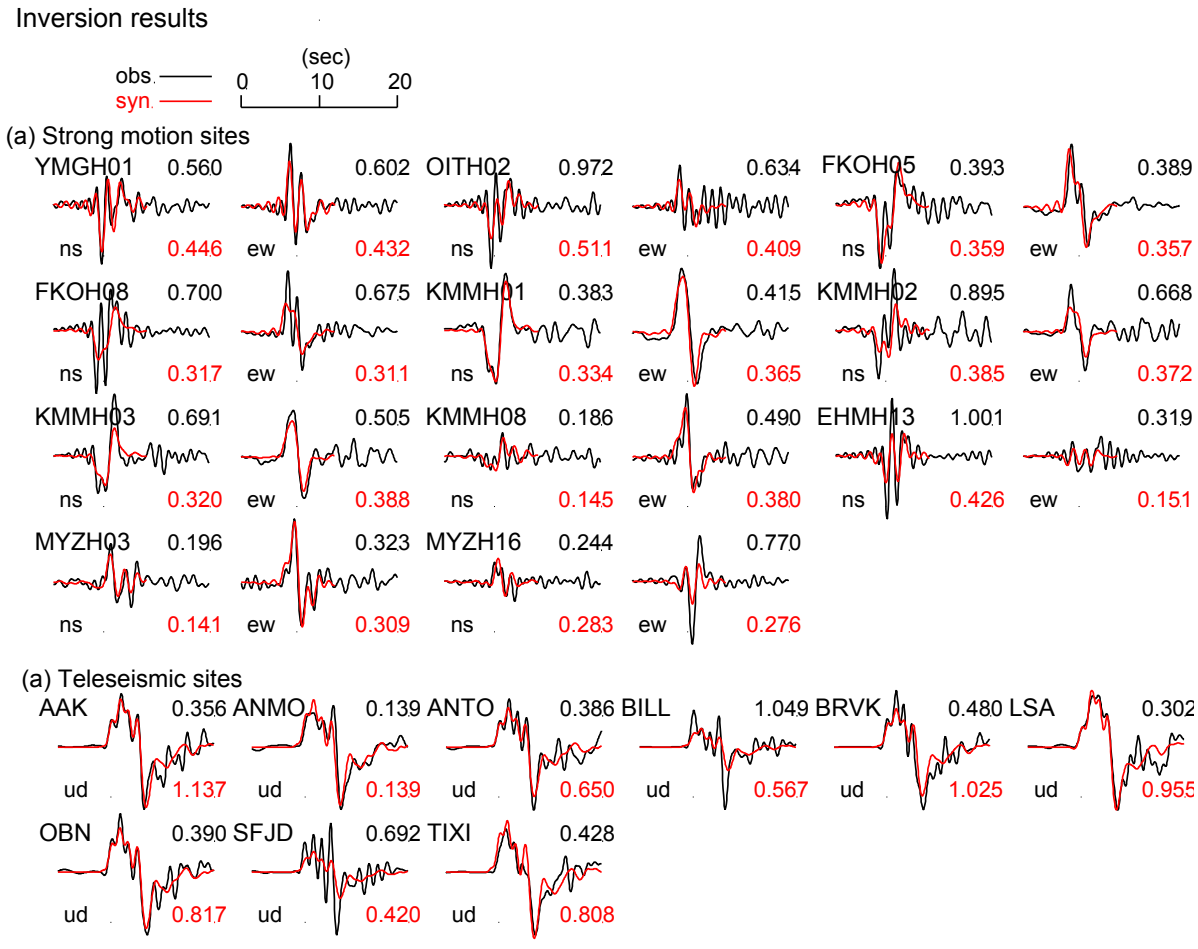

Figure 4 Comparison of observed waveforms (black) with synthetic waveforms (red).

Figure 5d shows snapshots of slip velocity at peak time of 4 pulses in the moment rate function. Though slip velocity is emitted from some portions, large slip velocities are located in and around the portion with large slip in Figure 5c. First pulse in the moment rate function is emitted from the portion just above the hypocenter. And the others are emitted from the portion about 8 km shallower from the hypocenter. As the whole, rupture propagated to shallower direction.

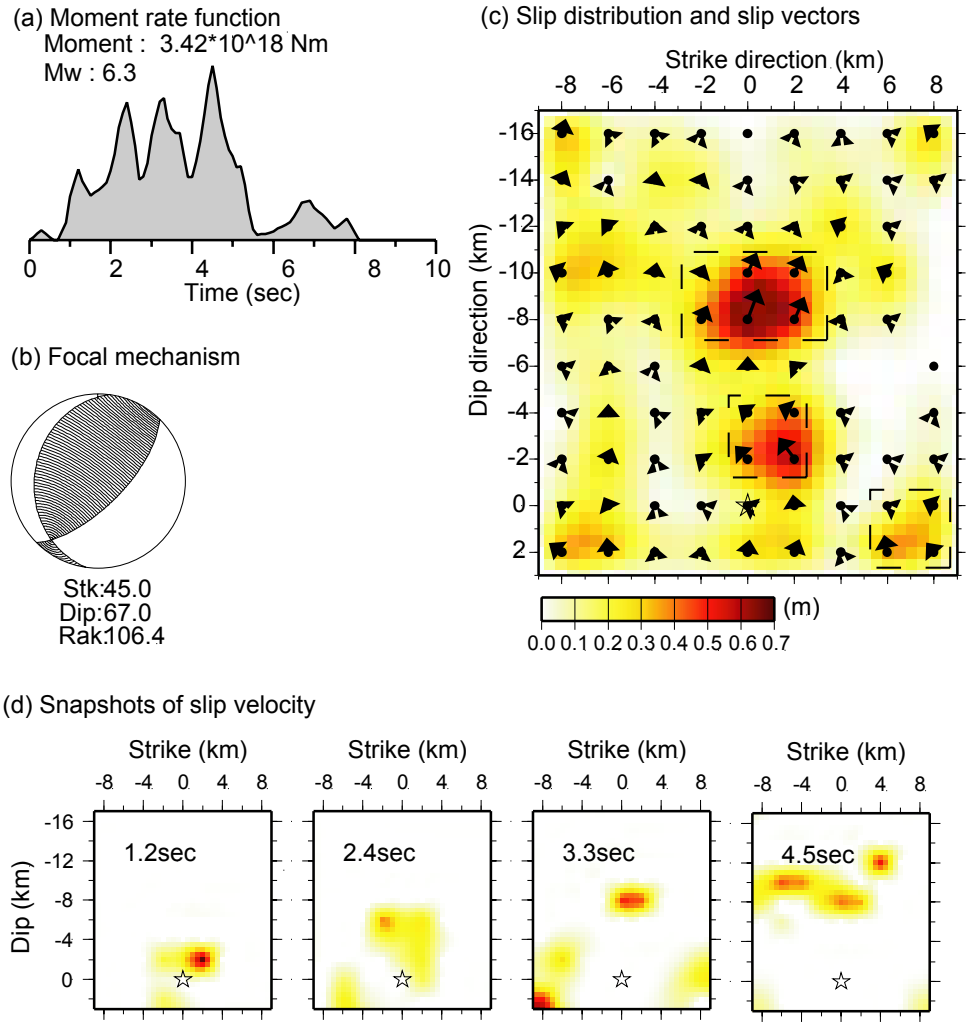

Figure 5 (a) Total moment rate function, (b) Focal mechanism projected on the lower hemisphere, (c) slip distribution and slip vectors, (d) snapshots of slip velocity at 1.2 sec, 2.4 sec, 3.3 sec and 4.5 sec. Star indicates the hypocenter in Figs. 5(c, d). Portions satisfied the asperity criterion by Somerville *et al.* (1999) are surrounded by broken line in Fig. 5(c).

We try to extract asperities from our results by applying a standard criterion by Somerville *et al.* (1999). Three portions satisfy this criterion, which are showed in Figure 5c. One is just above the hypocenter and other one is about 8km shallower from the hypocenter, the other is located at right-side lower corner. Judging from rupture propagation direction, we conclude that the slip at right-side lower corner may be an artifact produced by the systematic error of our inversion. Then we do not regard this portion as asperity. The second asperity may consist of three small asperities. The resultant seismic moment of each asperity is 4.59 x 10^{17} Nm and 7.59 x 10^{17} Nm, respectively. Combined asperity area is 40 km^2, which is comparable to the area deduced from the empirical relation of crustal earthquake by Somerville *et al.* (1999). The asperity area estimated in this study may be somewhat larger.

4. SHORT PERIOD LEVEL OF SOURCE SPECTRUM

4.1. Estimation Method

S-wave acceleration source spectrum $M(f)$ is written by following form.

$$M(f) = \frac{4\pi\rho_s\beta_s}{R_{\theta\varphi}} \frac{R^{\gamma} O(f)}{G(f)} \exp\left(\frac{\pi f T_s}{Q_s(f)}\right) \sqrt{\frac{\rho_g\beta_g}{\rho_s\beta_s}} \tag{4.1}$$

where $O(f)$ is observed S-wave acceleration spectrum, $G(f)$ is site amplification, R is hypocentral distance, T_s is travel time of S-wave, $Q_s(f)$ is Q-value of S-wave, ρ and β are density and S-wave velocity (subscription s and g indicate source and site). Last term of Eqn. 4.1 is for the correction of the different acoustic impedance. $R_{\theta\phi}$ is radiation pattern. We assume the site amplification as logarithmical average of one dimensional theoretical amplification between SH and SV waves. In the calculation of the amplification function, we use geological structure based on boring information and incident angle is calculated using JMA table at each site. S-wave travel time is referred to JMA travel time table. In this study we operate two horizontal component data independently, then we assume $R_{\theta\phi}$ as the value of radiation pattern 0.63 (Boore and Boatwrite, 1984) divided by the square root (Satoh, 2004). Other parameters are listed in Table 4.1. S-wave velocity at each site is based on boring information.

Table 4.1 Parameter setting for estimating source spectrum

γ	ρ_g	β_g	ρ_s	β_s	Q_s*
1.0	2.3-2.5 g/cm^3	1.58-3.00 km/s	3.2 g/cm^3	4.62 km/s	$114f^{0.69}$

* Evaluated by Kawase and Matsuo (2004)

4.2. Results

In this study we select stiff sites with a epicentral distance less than 100km. We exclude back-arc sites from the analysis because of the strong attenuation of short-period seismic waves in the mantle wedge. Finally we select three sites. Calculated source spectra are shown in Figure 6a. Each spectrum grows in proportion to second power of frequency in the frequency range lower than 2 Hz and become flat from 2 to 10 Hz at each site. We calculate logarithmic average in this range as the short period level. Figure 6b shows the results of each component. Finally we calculate logarithmical average level of each component. Estimated short period level is 3.51 x 10^{19} Nm/s^2. We compare this value with the results from other intraslab events (Maeda, 2003; Morikawa and Sasatani, 2004; Satoh, 2004) in Figure 7. In the figure the empirical relations of intraslab earthquake (Satoh, 2004) and crustal and interplate earthquake (Dan et al., 2001) are also shown. These relations show that the short period level of intraslab earthquake is higher than that of crustal and interplate earthquake. Our result is consistent with those of other intraslab events. This high short period level may be related to the complex source process shown in this study.

5. CONCLUSION

We investigate source characteristics of 2006 the Oita-chubu earthquake. First we perform waveform inversion to estimate spatio-temporal slip distribution. The results showed complex source process. We apply standard criterion by Somerville *et al.* (1999) to the inversion result and extract two asperities. Our results suggest the second asperity may consist of three small asperities. Next we estimate short period level. Estimated short period range is 3.51 x 10^{19} Nm/s^2, which is consistent with typical level estimated from other intraslab events.

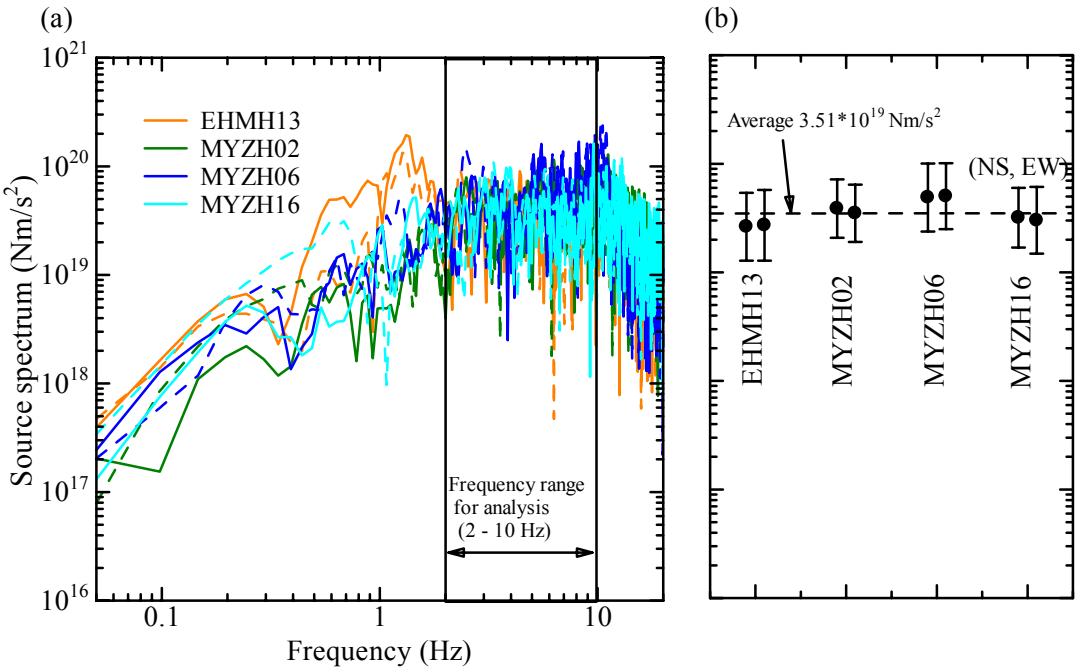

Figure 6 (a) S-wave acceleration source spectrum and (b) short-period level estimated at each site.

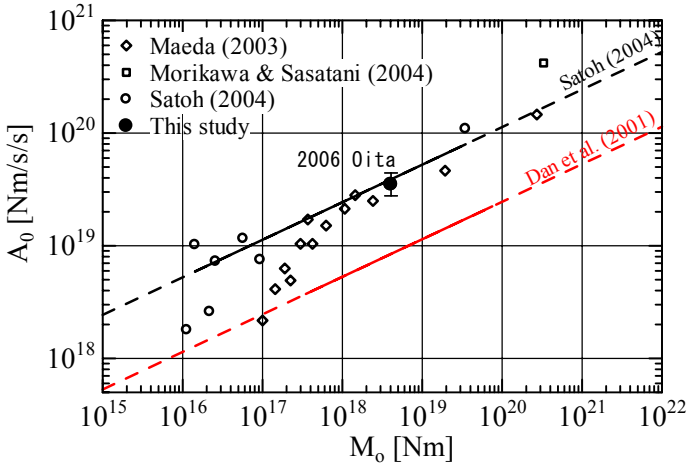

Figure 7 Comparison of estimated short-period level in this study with those of other intraslab events. Black and red lines indicate empirical short period level relation for intraslab earthquake (Satoh, 2004) and for crustal and interplate earthquake (Dan *et al.*, 2001), respectively.

ACKNOWLEDGEMENTS

We would like to thank National Research Institute for Earth Science and Disaster Prevention (NIED) for the strong motion data (K-NET and KiK-net), Management Center of the Incorporated Research Institutions (IRIS-DMC) for broadband data, the Japan Meteorological Agency (JMA) for hypocenter catalog and the Harvard University CMT Project for moment tensor solution catalog. We used the Generic Mapping Tools (Wessel and Smith, 1998) to draw some of figures in this paper.

REFERENCES

Akaike, H. (1980). Likelihood and the Bayes procedure, in *Baysian Statics*, edited by J. M. Bernardo et al., pp. 143-166, University Press, Velencia, Spain.

Bouchon, M. (1981). A simple method to calculate Green's functions for elastic layered media. *Bulletin of the Seismological Society of America* **71**, 959-971.

Boore, D. M. and Boatwright, J. (1984). Average body-wave radiation coefficient. *Bulletin of the Seismological Society of America* **74**, 1615-1621.

Dan, K., Watanabe, T., Sato T. and Ishii, T. (2001). Short-period source spectra inferred from variable-slip rupture model and modeling of earthquake faults for strong motion prediction by semi-empirical method. J*ournal of Structural and Construction Engineering* **545**, 51-62 (in Japanese with English abstract).

Fukahata, Y., Yagi, Y. and Matsu'ura, M. (2002). Waveform inversion for seismic source process using ABIC with two sorts of prior constraints: Comparison between proper and improper formulations. *Geophysical Research Letters* **30**, 10.1029/2002GL016293.

Heartzell, S. H. and Heaton, T. H. (1983). Inversion of strong ground motion and teleseismic waveform data for the fault rupture history of the 1983 Imperial Valley, California. Earthquake. *Bulletin of the Seismological Society of America* **73**, 1553-1583.

Kanamori, H. and Stuwart, G. S. (1976). Model of the strain release along the Gibbs fracture zone, Mid Atlantic ridge. *Physics of the Earth and Planetary Interiors* **11**, 312-332.

Kawase, H. and Matsuo, H. (2004). Separation of source, path and site effects based on the observation data by K-NET, KiK-net, and JMA strong motion network. *Journal of JAEE* **4**, 33-52 (in Japanese with English abstract).

Maeda, T. (2003). A study on characteristics of seismic wave attenuation and seismic sources in the subduction zone. Doctor thesis, Hokkaido University.

Morikawa, N. and Sasatani, T. (2004). Source models of two large intraslab earthquakes from broadband strong ground motion. *Bulletin of the Seismological Society of America*, **94**, 803-817.

Okada, Y., Kasahara, K., Hori, S., Obara, K., Sekiguchi, S., Fujiwara, H. and Yamamamoto, A. (2004). Recent progress of seismic observation networks in Japan - Hi-net, F-net, K-net and KiK-net -. *Earth Planets Space* **56**, xv-xxviii.

Satoh, T. (2004) Short-period spectral level of intraplate and interpolate earthquakes occurring off Miyagi Prefecture. *Journal of JAEE* **4**, 1-4 (in Japanese with English abstract).

Somerville, P. G., Irikura, K., Graves, R., Sawada, S., Wald, D., Abrahamson, N., Iwasaki, Y., Kagawa, T., Smith, N. and Kowada, A. (1999). Characterizing crustal earthquake slip models for the prediction of strong ground motion. *Seismological Research letters* **70**, 59-80.

Takeo, M. (1985) Near-field synthetic seismograms taking into account the effects of anelasticity - The effects of anelastic attenuation on seismograms caused by a sedimentary layer -. *Papers in Meteorology and Geophysics* ***36***, 245-257 (in Japanese with English abstract).

Wessel, P. and Smith, W. H. F. (1998). New improved version of the generic mapping tools related. *Eos Tranactons American Geophysical Union* **79**, 579.